Photoactive Anthraquinone-Based Host-Guest Assembly for Long-Lived Charge Separation

Ajay Jha,[‡1] Kaustubh R. Mote,[2] Suman Chandra,[†3] Perunthiruthy K. Madhu[2] and Jyotishman Dasgupta[1*]

[1]*Department of Chemical Sciences, Tata Institute of Fundamental Research, Homi Bhabha Road, Colaba, Mumbai 400005 , India.*

[2]*TIFR Center for Interdisciplinary Sciences, Tata Institute of Fundamental Research Hyderabad, 36/P Gopanpally Village, Serilingampally Mandal, RR District, Hyderabad 500046, India.*

[3]*Physical/Materials Chemistry Division, CSIR-National Chemical Laboratory, Dr. Homi Bhabha Road, Pune 411008, India.*

[‡]Present address: *The Rosalind Franklin Institute, Rutherford Appleton Laboratory, Harwell Campus, Didcot, Oxfordshire, OX11 OFA, UK.*

[†]Present address: *Technische Universität Berlin, Hardenbergstrasse 40, 10623 Berlin, Germany.*

*****Corresponding author email: dasgupta@tifr.res.in

Abstract

Porous 2D-covalent organic frameworks (COF) that are assembled axially through weak π-stacking interactions can provide reticular charge transport channels while playing host to kinetically stabilized reactive molecular redox-states. Here we demonstrate the above paradigm by constructing a host-guest supramolecular charge transfer (CT) assembly using photoactive anthraquinone-based crystalline COF as an acceptor while incarcerating electron donor N,N-dimethylaniline (DMA) inside it. Employing femtosecond broadband transient absorption spectroscopy in combination with electron paramagnetic resonance (EPR) studies, we show that the CT occurs rapidly within <110 femtoseconds after photoexcitation, subsequently leading to long-lived charge separation with 13% quantum efficiency at room temperature. Photoinduced EPR signature of the long-lived confined DMA cation radical confirms the disparate regions of charge localization while ^{1}H-^{13}C correlation experiments using solid-state NMR spectroscopy enumerate the packing of the amines inside the host-guest COF assembly. Our work demonstrates the potency of rationally designed charge transport pathways in supramolecular assemblies for efficient charge separation which if optimally tuned should pave the way for COF-based photocatalytic reaction centres.

INTRODUCTION

Optimization of photoinduced charge generation is a critical step towards the development of efficient photovoltaics[1, 2] as well as robust photo-catalysts.[3] Taking inspiration from photoinduced charge transfer in membrane-bound macromolecular superstructures i.e. photosystems in natural photosynthesis, a large number of artificial molecular structures from complex supramolecular assemblies[4-9] to polymers[10, 11] have been synthesized over the past decade. To achieve the desired photon-to-charge conversion efficiency within molecular frameworks, chemists have built hierarchical structures using a combination of direct covalent functionalization along with weak but directional interactions such as H-bonds, π-π stacking etc.[12-14]

Two-dimensional (2D) covalent organic frameworks (COFs) with effective porosity have shown great potential for application in organic electronics apart from their utilization in gas storage, separation and catalysis.[15-28] Photoactive COFs have recently been employed to form columnar arrays using desired π-conjugated networks for charge generation. The strong electronic coupling between eclipsed 2D organic polygon sheets is achieved through π-clouds that impart three-dimensional ordered networks creating one-dimensional linear charge transport channels. In fact, recent studies have revealed large exciton diffusion coefficients in 2D COFs.[29, 30]

To achieve charge generation in these structures, either the donor-acceptor (DA) molecular building blocks were engineered into the walls[21, 31-45] or open lattices were filled with large fullerene acceptors using covalent attachment with the donor decorated frameworks.[46] In a seminal work, Ihee and colleagues elucidated phonon-assisted ultrafast polaron pair (or radical pair) formation in 2D DA COF.[47] Although covalent linkage of donor and acceptor molecules do create well defined molecular interfaces for charge transfer (CT), the strong electronic coupling amongst photogenerated charge pairs renders high electrostatic barriers for generation of free charges. Alternatively, donor mounted porous COF structures have also been employed as hosts incarcerating bulky fullerene-based acceptors

as guest molecules to execute photo-induced charge generation process. Remarkably, a photovoltaic cell based on crystalline phenazine-linked CS-COF and [6,6]-phenyl-C_{61}-butyric acid methyl ester (PCBM) was reported with a modest power conversion efficiency of 0.9%.[48] Although the design proved to have low photovoltaic efficiency, the fascinating concept of utilizing host-guest chemistry for charge generation and possibly redox catalysis[49] with long-lived radical states is extremely alluring.

Elaborating on the host-guest idea, we propose that tuning the efficiency of charge transport in the crystalline COF framework subsequent to photoinduced charge transfer will enable supramolecular designs conducive for confined photocatalysis. Earlier work showed that ultrafast charge transfer can be triggered from organic amines after photoexciting visible-light absorbing anthraquinone moieties,[46] organic chromophores that can potentially stabilize multiple redox states. Critical evaluation of the rates revealed that the out-of-plane deformation modes of the anthraquinones drive the CT reaction. However the major drawback arose from the short-lived CT state due to fast recombination in the anthraquinone:N,N-dimethylaniline (DMA) π-stacked pair within ~10-15 ps thereby limiting its utility for catalytic chemistry.[50] To induce the long-lived charge separation in such D-A pairs, charges have to be separated rapidly by an efficient hopping mechanism thereby localizing them spatially over different regions of the conjugated framework.

Guided by the idea of normal mode engineering[50] wherein the potent driving modes can be harnessed by improvising the molecular topology, we hypothesized that a 2D anthraquinone-based COF structure with uniform stacking along the z-direction would be optimal for rapid charge transport assisted by the sheet deformation modes (see Figure 1). To demonstrate this we designed charge transfer (CT) inclusion complex of a small organic amine donor with the electron accepting anthraquinone COF framework. We chose 2D β-ketoenamine-linked DAAQ-TFP COF as the photo-oxidant host, first synthesized by Dichtel and co-workers

through condensation of redox-active monomer 2,6-diaminoanthraquinone (DAAQ) with 1,3,5-triformylphluroglucinol (TFP).[51] We incarcerated DMA molecules to test our hypothesis of efficient charge generation using a non-covalent CT assembly of DMA:COF complex. Employing broadband femtosecond transient absorption spectroscopy complemented with photoinduced EPR measurements, we captured the optical signatures of long-lived charges after subjecting the non-covalent assembly of COF and DMA to photoexcitation. Population analysis from transient kinetic data revealed internal quantum yield of 13 % for charge separation which is limited by the presence of fast recombination pathway of ~1.7 ps. Two dimensional NMR experiments with ^{1}H-^{13}C correlations in the solid-state provided a molecular view of the host-guest interactions.

Experimental Section

Chemicals. N,N-dimethylaniline (DMA) was purchased from SD Fine Chemicals (P) Ltd. and distilled before use. 1,3,5-triformylphloroglucinol was prepared from Phloroglucinol using literature procedure.[52] All other reagents and solvents were commercially available and used as received.

Synthesis of DAAQ-TFP COF. TFP (0.3 mmol, 63 mg) and DAAQ (0.45 mmol, 107 mg) were added into a pyrex glass ampoule (i.d x o.d = 0.9 mm x 1.2mm; height = 24 cm) with N,N-dimethylacetamide (DMAc, 3 mL) as solvent and sonicated for 15 min. After sonication, acetic acid (6M, 0.5 mL) was added and again sonicated for 10 min. The whole reaction mixture was flash frozen in liquid nitrogen and kept under partial vacuum (100 mTorr). After three cycle of freeze pump through, the ampoule was vacuum sealed and heated at 90 °C for 2 day. The COF was collected by filtration as red-orange precipitate and purified by washing with DMAc (until the filtrate was colorless), followed by water and finally with acetone. The pure DAAQ-TFP COF (75% yield) was activated at 120 °C in a dynamic vacuum for 12 h. Anal. Calcd. For ($C_{60}H_{30}N_6O_{12}$): C, 70.12; H, 2.99; N, 8.13. Found C, 65.54; H, 3.48; N 8.01.

Powdered X-ray diffraction measurements: Powder X-ray diffraction (PXRD) patterns were recorded on a Rigaku, MicroMax-007HF with high intensity Microfocus rotating anode X-ray generator. All the samples were recorded in the (2θ) range of 2–40 degrees and data was collected with the help of Control Win software. A Rigaku, R-axis IV++ detector was employed in wide-angle experiments. The radiation used was Cu Kα (1.54 Å) with a Ni filter, and the data collection was carried out using an aluminium holder.

Gas adsorption measurements. All gas adsorption experiments (up to 1 bar) were performed on a *Quantachrome Quadrasorb* automatic volumetric instrument.

Steady state absorption measurements. Diffuse reflectance measurements of DAAQ-TFP COF and DMA⊂DAAQ-TFP COF films were performed in JASCO V-530 equipped with a diffuse reflectance auxiliary and were referenced to $BaSO_4$.

IR Measurements. Fourier transform infrared (FTIR) spectra of the samples were recorded on a JASCO FT/IR- 4100 spectrometer. Fourier transform infrared (FT-IR) spectra were taken on a Bruker Optics ALPHA-E spectrometer with a universal Zn-Se ATR (attenuated total reflection) accessory in the 600-4000 cm^{-1} region or using a Diamond ATR (Golden Gate).

Solid-state NMR measurements. All experiments were done on a 16.5 T Bruker magnet with fully packed 2.5 mm rotors at the magic-angle-spinning frequency of 27737 Hz. Sample temperature was regulated to have an effective sample temperature of 40 ± 5 ^{o}C. ^{13}C-cross-polarization experiment was done by keeping the ^{13}C radio-frequency (RF) amplitude at 40 kHz and optimizing the ^{1}H RF amplitude to achieve the second side-band matching condition (~95 kHz). Contact time of 2 ms was used. 100 kHz SW_f-TPPM[53] decoupling was used on ^{1}H during acquisition. 25600 transients were averaged with a recycle delay of 2 s for both the samples.

^{1}H-^{13}C correlation experiment was done using 100 kHz supercycled phase-modulated-Lee-Goldburg (PMLG) homonuclear decoupling during ^{1}H evolution.[54] 640 transients were acquired for each of the 32 indirect points so as to give a final ^{1}H chemical shift evolution time

of 2.93 ms. The ^{1}H dimension was rescaled using the chemical-shift scaling factor of 0.549 for PMLG.

For the mixed sample, the ^{1}H-^{13}C correlation experiment with an additional spin diffusion element was recorded to establish inter and intra-molecular correlations. This was achieved by reverting the ^{1}H magnetization to the Z-axis after ^{1}H chemical shift evolution and inserting a delay of 25 ms (which serves to exchange the magnetization amongst protons). This was followed by another 90^{o} pulse which brought the ^{1}H magnetization to the transverse plane. This was followed by cross-polarization to ^{13}C and detection as in the previous case.

COF and DMA⊂DAAQ-TFP COF films preparation. DAAQ-TFP COF and DMA⊂DAAQ-TFP COF films were fabricated over quartz substrate. Briefly, a hot piranha solution (mixture of 96% H_2SO_4 and 30% H_2O_2 in a 2:1 v/v ratio) was used to clean UV-transparent quartz substrate of 2.5 cm. The cleaned quartz substrate was rinsed with deionized water and then dried in an oven at 120 °C for 2 hrs. The dried substrate was subsequently treated with UV generated ozone for 1 hr. COF solutions were prepared by suspending 4 mg of the mechanically grinded solid powder material in 1 ml of methanol. The dispersed COF solutions were drop-casted on the cleaned quartz substrate and then dried under argon atmosphere at 50 °C. The dried film was cooled to room temperature and then sealed under argon using another cleaned square quartz substrate using epoxy resin at the edges. The film thickness of ~1.4 μm was characterized using Zeta microscopy set up which provides 3D profile of film over substrate. Sample for this profiling is prepared by scratching the portion of the COF film from the substrate. Analysis of the step height from substrate to COF film in 3D profile provides information on film thickness as shown in Figure S2, supporting information.

***fs*-transient absorption measurements.** All pump-probe measurements were carried out using transient absorption spectrometer as described before.[55] Briefly, the output of Ti:Sapphire laser-based oscillator (Coherent Micra-5 Modelocked Titanium: Sapphire Laser system) was 380 mW with bandwidth of ~100 nm and 80 MHz repetition rate. The output of

the oscillator was amplified to ~4 mJ/30 fs at 1 kHz repetition rate using chirped pulse amplification (Coherent Legend Elite amplifier laser system). The amplified fundamental beam is divided by a 50:50 beam splitter to generate the pump and probe pulses. The 490 nm pump pulse was produced using an optical parametric amplifier (Coherent OPeraASolo Optical Parametric Amplifier system) and attenuated to 8-10 μJcm^{-2} pulses with >250 μm beam size at the focus. To vary the time delay between pump and probe pulses, the path length of the pump beam was controlled through a quadra-pass mirror assembly (Newport). For all the measurements, polarization of the pump pulse was kept at magic angle (54.7°). The second portion of the fundamental 800 nm amplified beam was attenuated by iris and neutral density filter before focusing it on a 2 mm thick sapphire crystal to achieve stable probe from 400-1400 nm. After passing through the sample, probe beam was channeled to a multichannel detector procured from Ultrafast Systems, Sarasota USA as part of the Helios® spectrometer in which probe beam was dispersed onto detector array (291 pixels for visible and 93 pixels for NIR) after entering through the spectrograph. Visible and NIR part of the continuum were separated using low pass (at 750 nm) and high pass (at 830 nm) filters respectively. The instrument response function (IRF) of ~110 fs was measured using optical Kerr-effect (OKE) arrangement on a 1 mm thick glass with λ/4 polarizer (in pump path) and an analyzer (in the probe path). To avoid bimolecular decay processes, measurements were carried out in the linear excitation regime (Figure S3a). To check the stability of the film, experiment was again repeated on the same focal spot and kinetic data for these measurements were compared (Figure S3b). Measurements were also performed on different spots on the film which showed the similar kinetics. An extended analysis of the transient spectra has been performed which involves chirp correction and kinetic analyses. Chirp correction was performed using commercial Surface Xplorer® software. The kinetic analyses at different wavelengths were carried out using IGOR pro 5 with programs written to deconvolve the decay time-constants from the IRF.

Photoinduced EPR measurements. Photoinduced EPR spectra of both the DAAQ-TFP COF and DMA⊂DAAQ-TFP COF were recorded in a TE011 cavity on a Bruker EMX Micro X-band spectrometer. All the measurements were performed at room temperature with operating frequency at 9.31 GHz. For all the measurements the samples were degassed to remove oxygen. For recording the EPR spectra, MW power of 0.2 mW was found to be optimal with modulation amplitude of 1 Gauss at 100 kHz modulation frequency. The illumination in the visible range was done using a Xenon lamp with a UV filter while the power was kept at ~10 W focused on to the frozen sample through a transparent window of 5 mm size. Both dark and illuminated spectra were recorded separately. Post illumination the sample was re-measured in the dark to check for the reversibility and was found to be intact.

Results and Discussion

Synthesis of DAAQ-TFP COF: The DAAQ-TFP COF was synthesized by Schiff-base condensation reaction of 1, 3, 5-triformylphloroglucinol (TFP) and 2, 5-diamino anthraquinone (DAAQ) via solvothermal method as reported in the literature.[51] The formation of β-keto-enamine was proved by the presence of C=O, C=C and C-N stretching frequency at 1618, 1560 and 1248 cm-1 respectively in FTIR (Figure S1a, supporting information). The absence of aldehydic (C-H) and amine (N-H) stretches suggested the conversion of reactants into product as DAAQ-TFP COF. The extra C=O stretch at 1664 cm-1 was due to the anthraquinone unit in the COF structure. The PXRD of the DAAQ-TFP COF was performed to check the crystallinity. The low angle peaks at $2\theta = 3.3, 6.0, 7.4$ and 27° corresponds to the (100), (110), (210) and (001) reflections respectively of a 2-D hexagonal layered network in nearly eclipsed stacking arrangement (Figure S1b, supporting information). The permanent porosity and the surface area were calculated from the N2 adsorption isotherm at 77 K. The surface area was very much affected by the reaction conditions (solvent mixtures and temperature) and purification and/activation method as reported by the Ditchel group.[51] The type-I isotherm

suggests the micro porous nature of this COF. The average BET surface area of DAAQ-TFP COF was 398 m2g-1 with an average pore diameter in the range of (11-19) Å (Figure S1c and S1d, supporting information), calculated from nonlocal density functional theory (NLDFT), little smaller than theoretical pore diameter (23 Å) suggesting a little extent of displacement of the layers. This was also confirmed by the broad (001) reflection at $2\theta = 27°$ in the PXRD of DAAQ-TFP COF.

Characterization of DMA⊂DAAQ-TFP COF inclusion complex: Incarceration of the DMA molecules inside the crystalline COF material was achieved by incubating solid powder of the COF in DMA for two weeks in dark. The inclusion complex so formed was filtered and dried. Powder-XRD measurements reveal the preserved crystallinity in the inclusion complex as shown in Figure 2*b*. Colour of the inclusion complex changed to black as compared to brick red color of the only DAAQ-TFP COF sample as shown in the inset of Figure 2*a*. The absorption spectrum in the reflection mode using the diffuse reflectance set up also showed the presence of new absorption bands for the inclusion complex which are red-shifted with respect to the empty COF absorption feature, as shown in Figure 2*a*. DMA⊂DAAQ-TFP COF inclusion complex was characterized for the presence of DMA using different spectroscopic techniques. IR spectrum of the inclusion complex showed a new feature at 1348 cm^{-1} which is a characteristic region of aromatic *tert*-amines C-N stretch coming from guest DMA molecules, shown in Figure 2*d*. To confirm the inclusion of DMA molecules in the COF network, solid state ^{13}C-NMR was performed. Details of the NMR experiment have been discussed in the experimental section. A distinct peak of alkyl carbon at $\delta = 40$ ppm highlights the presence of DMA alkyl-carbon. In the aromatic region of the DMA□DAAQ-TFP COF spectrum, peak at $\delta = 133$ ppm is from β-carbons in the DMA while the peaks at $\delta = 116$ and 127 ppm correspond to α- and γ-carbons of the DMA, respectively. The aromatic carbon linked to N-atom should be the most deshielded and is expected to be at ~150 ppm, overlapped with the intense signals from ANQ framework. In addition, ^{1}H-NMR of the recovered DMA after

being extracted from the DMA⊂DAAQ-TFP COF shows all characteristic features DMA which confirms the reversibility and stability of the COF:DMA inclusion complex. Thus, solid-state NMR and IR data confirm the presence DMA in the inclusion complex which is examined for its optical properties as discussed in the following sections.

^{1}H-^{13}C correlation solid-state NMR experiments. In order to characterize the nature of DMA incarceration inside the anthraquinone COF stacks, we carried out ^{1}H-^{13}C correlation through solid-state NMR of the pure COF and the DMA⊂DAAQ-TFP COF powder. We were able to identify distinct chemical shifts for the backbone of the ANQ moiety in the ^{1}H-^{13}C correlation spectrum as shown in Figure 5*a*. In presence of DMA, a peak resolved in both the ^{1}H and ^{13}C dimensions was identified as belonging to the -CH_3 groups attached to the -$N(CH_3)_2$ group (1' peak in Figure 5*b*). Based on known ^{13}C-NMR spectrum of DMA[56], we assigned some of the overlapping peaks in the ^{1}H -^{13}C correlation spectrum of the mixed sample to the meta, ortho and para positions of DMA. Interestingly when an additional ^{1}H-^{1}H mixing period was included after ^{1}H evolution, correlation peak between the methyl-amine of the DMA and the 2 position (~135 ppm) of the DAAQ-TFP COF moiety is observed (shown in Figure 5*c*). The correlation peak at ~110 ppm most likely indicates the connectivity to the 2' peak of DMA itself. Additionally, a possible correlation with the 1 position of DAAQ-TFP COF moiety (~145 ppm) with the N-methyl group of DMA is also observed. These correlations suggest that the methyl groups are in close proximity to 2- and also possibly 3- position protons of the ANQ. Based on NMR, a model for the DMA⊂DAAQ-TFP COF complex is proposed in which the amine group is pointing directly towards carbonyl carbon of the DAAQ-TFP COF as shown in Figure 5*d*, which agrees with the observed proximity to the 2 position of anthraquinone. Additionally we do not observe polymerization of the incarcerated DMA molecules even after photo-irradiation or keeping it for a long time in the dark. These arguments support the structural model in which all the phenyl groups of the incarcerated DMA molecules are

hydrophobically packed in the interior of the COF while the amine part directly points towards the COF walls.

Steady-state absorption measurements. Steady state absorption spectra of DAAQ-TFP COF and DMA⊂DAAQ-TFP COF inclusion complex for thin films obtained by diffuse reflectance clearly show new features at ~645 and ~800 nm in comparison to COF only spectrum featuring broad peak at ~550 nm, as shown in Figure 2*a*. The flat optical band in the blue-side between 400 to 450 nm is partially caused by light scattering. In a previous study, we had reported charge transfer (CT) band for 1-amino-4-hydroxyanthraquinone-DMA complex at 650 nm.[50] Using this observation, we conjectured the new peak at ~645 nm for the inclusion complex to be of CT character. In addition to this feature, the other new peak at ~800 nm probably refers to the delocalised CT excitation over DMA⊂DAAQ-TFP COF inclusion complex. Dincã and co-workers have also reported the formation of CT complexes for thiophene based COF with tetracyanoquinodimethane (TCNQ) which showed distinct CT band at ~850 nm.[57] Therefore, our steady state absorption data supports the existence of incarcerated DMA molecules as CT inclusion complex within the COF framework.

***fs*-Transient absorption measurements.** In order to track the reactivity of these inclusion complexes for photoinduced charge generation, we carried out femtosecond transient absorption (TA) spectroscopy upon 490 nm photoexcitation with 8-10 μJ/cm^2 pulses and ~250 μm beam size at the focus. Absorption transients for DAAQ-TFP COF and DMA⊂DAAQ-TFP COF thin films were recorded at different pump-probe delays in the two different probe windows ranging from 500-750 nm and 830-1200 nm with an IRF of ~110 fs. Details of the thin film preparation methodology and TA experiment have been mentioned in the materials and methods section. The TA measurements were performed in the linear excitation regime to avoid bimolecular decay processes which was established by pump power dependence of transient signals as shown in Figure S3, supporting information. The evolution of ground state bleach (GSB) and stimulated emission (SE) features for DAAQ-TFP COF thin film is shown

in Figure 3*a*. The distinct transient features at ~530 nm and ~680 nm correspond to GSB and SE respectively. In the NIR probe window of 800-1300 nm, spectral traces show an instantaneous positive broad absorption feature centered at 1040 nm (in Figure 3a) after photo-excitation which possibly represents the DAAQ-TFP COF singlet exciton absorption spectrum. This singlet exciton feature along with GSB and SE features subsequently decay away as shown by 2 ns trace.

TA measurements on thin film of DMA⊂DAAQ-TFP COF inclusion complex on the other hand show a broad excited state absorption (ESA) centering at ~630 nm masking GSB signature which does not decay within the experimental time delay of 2 ns, as shown in Figure 3*b*. TA measurements on CT complexes with anthraquinone derivatives have shown that anthraquinone anion radical, $ANQ^{\bullet-}$ absorbs at ~640 nm which closely resembles the observed 1 ps transient of DMA⊂DAAQ-TFP COF inclusion complex thin film (black trace in Figure 3*b*).[50, 58] However, the feature is broader especially at the red edge which is caused possibly due to two reasons. Firstly, DAAQ molecule is attached to a conjugated network making the anion radical chemically heterogenous as it will delocalize over the framework. In addition, it may as well indicate the charge migration through the stacked anthraquinones in the supramolecular aggregate.[8] Previously reported work on perylene diimide (PDI) based superstructures have shown that aggregation induced charge migration broadens the absorption feature of perylene diimide radical anion, $PDI^{\bullet-}$.

The second possible reason for the broad absorption feature for $ANQ^{\bullet-}$ could be the presence of overlapping DMA cation spectral trace in NIR probe window for 1 ps time point shows structured positive excited state absorption band with features centered at ~860 nm and ~1025 nm, as shown in Figure 3*b* (black trace). Therefore this excited state absorption band is a convolution of the singlet exciton absorption spectrum of DAAQ-TFP COF along with the new feature(s) arising from the interaction with incarcerated DMA molecules. In classical CT complexes, the formation of radical ion pair is mediated by the photo-excited coupled CT state,

$[D^{\bullet+}\text{--}A^{\bullet-}]^*$.[59] Previously reported work on host-guest complexes of $Pd_6L_4^{12+}$ cage and 9-anthracenealdehyde have shown the simultaneous photogeneration of $[D^{\bullet+}\text{--}A^{\bullet-}]^*$ state alongwith the radical ion pair state.[60, 61] Thus, we conjecture that the lower energy transitions in transients of DMA⊂DAAQ-TFP COF inclusion complex possibly have a contribution from the $[D^{\bullet+}\text{--}A^{\bullet-}]^*$ state. The appearance of $ANQ^{\bullet-}$ and $DMA^{\bullet+}$ along with the $[D^{\bullet+}\text{--}A^{\bullet-}]^*$ state after photo-excitation provides the unequivocal evidence for charge generation.

To enumerate the population dynamics and lifetimes of the states, single point kinetic analysis was performed. Kinetic analysis of the TA data at 732 nm for DAAQ-TFP COF thin film shows bi-exponential decay with the time constants of 13.2 ± 5.1 ps (80%) and 257 ± 93 ps (20%) as shown in Figure S4, supporting information. Thus, the average lifetime of the exciton in these frameworks is ~60 ps which is almost half as that for thienothiophene-based COF (exciton lifetime ~120 ps), reported by Bein and co-workers.[62] Shorter exciton lifetime of the DAAQ-TFP COF with lower bandgap could possibly be rationalized using energy gap law which invokes exponential increase in the non-radiative decay rate of multi-phonon processes with lowering of the bandgap.[63, 64] To confirm the exciton decay rate, kinetic analysis has been performed on singlet exciton absorption feature in NIR. Figure S4 in supporting information shows a kinetic trace averaged for probe window 893-907 nm. Similar to the GSB data, singlet exciton absorption also shows bi-exponential decay rates of 9.5 ± 2.1 ps and 157 ± 86 ps.

For DMA⊂DAAQ-TFP COF thin film, kinetic trace for $ANQ^{\bullet-}$ at 600-610 nm shows an IRF limited rise and bi-exponential decay with an ultrafast time-component of 1.7 ± 0.6 ps (87%) and a non-decaying component (>2 ns, 13%) as shown in Figure 4*a*. From the observed timescales, we infer that after excitation of the inclusion complex, an instantaneous charge transfer occurs which is followed by a fast recombination event of ~1.7 ps. But interestingly, 13% of the population does not decay within the timescale of the experimental pump-probe delay times of 2 ns. This shows that a fraction of population is able to do the charge separation

for long time. Kinetic analysis in the NIR window for 893-907 nm shows one distinct singlet exciton decay component of 75 ± 37 ps other than two components of 1.7 ps and non-decaying which are similar to the ones observed for $ANQ^{\bullet-}$ decay (Figure S6, supporting information). The simultaneous observation of IRF limited rise of $ANQ^{\bullet-}$ as well as exciton feature rules out the homogeneous kinetic model with excited state branching. Since excitation has been done where LE and CT transitions overlap, we argue for an inhomogeneous kinetic scheme to explain this kinetic data where optical excitation leads to independent formation of LE and CT states simultaneously. The populations in the CT state are further bifurcated into two different pathways, one leading to fast recombination of ~1.7 ps and other doing charge separation resulting into long-lived charges. The fast recombination of the charge pairs possibly arises due to poor coupling among some stacks for electron hopping.

EPR measurements. To establish unequivocal validity of the long lived charge generation in DMA⊂DAAQ-TFP COF inclusion complex, photoinduced EPR measurements were performed on DAAQ-TFP COF and DMA⊂DAAQ-TFP COF powder samples. At room temperature no steady state EPR signal was observed in the dark. Figure 4*b* shows photogenerated RT EPR signals of DAAQ-TFP COF and DMA⊂DAAQ-TFP COF samples while ensuring good insulation from O_2 gas. DMA⊂DAAQ-TFP COF shows a strong signal at g = 2.01 with distinct hyperfine splitting with coupling constant for $|a_{\text{H methyl}}|$= 4.7 Gauss for DMA cation radical.[65] On the other hand, DAAQ-TFP COF only spectrum did not show any photoinduced EPR signature. Thus, the room temperature photoinduced EPR signal for the DMA cation radical provides compelling evidence for generation of long lived charges from non-covalent host-guest assembly. In particular it should be noted here that the ability to observe localized DMA cation radical using a steady state light source emphasizes on the simplicity of our design principle.

The long-lived radical that was observed in both transient absorption and in the photoinduced EPR measnurements clearly indicate that the DMA cation radical could be harnessed as a catalytic moeity for carrying out confined reactions. In fact the idea of confining radicals to carry out catalysis has been demonstrated in nanocavities recently where the organic radicals stabilized inside confinement lend to reactivity in solution.[66] The fact that we observe the radical signatures of DMA at room temperature shows that the lifetime is long-lived enough to warrant diffusion based catalytic events. The advantage of putting these materials on electrodes will also enable redox events triggered by a volatge bias and hence has potential for many photoelectrochemical organic transformations.[67, 68]

CONCLUSION

In summary, we successfully demonstrate long-lived photo-induced charge separation in a porous anthraquinone-based COF assembly which can host electron-rich organic amines in its cavity. The design principle purely relies on optimal spatial ordering of the 2D-covalent-organic frameworks (COFs) stitched by weak π-stacking interactions along the z-direction, which allow for facile electron transfer between the conjugated sheets. Upon photo-triggering an ultrafast charge transfer reaction between visible absorbing anthraquinone-based COF host and incarcerated organic amine guest, we observed long-lived charges as characterized by optical and magnetic signatures of immediately formed cation and anion radicals. The extremely slow recombination time of the charges due to large spatial separation across the COF-stacks ensured that the EPR signature of the amine radical cation was easily identified by steady-state illumination at room temperature.

Our paradigm for prolonging charge separation can be generalized by simply choosing the complementary host-guest pairs to form rigid electron and hole transport channels. Based on these results we envision that photoactive COFs can be used to build artificial reaction centers that spatially separate electrons and oxidizing equivalents thereby mimicking natural

photosynthesis. The presented prototype can be suitably modified to support confined active sites for complementary oxidation and reduction photocatalytic reactions. Interfacing such structures with compatible electrode surfaces will allow for facile spatial separation of the two fuel generating reactions. In fact recent work has shown that anthraquinone COFs have great charge storage capacity,[62,63] and enabling our design principles should pave the way towards photon-efficient catalysis inside the pores.

ASSOCIATED CONTENT

Supporting Information. ANQ-COF characterization data, additional time-resolved data and details of the kinetic fitting parameters are provided.

ACKNOWLEDGMENT

Authors thank Dr. Kshama Sharma, TIFR Hyderabad for help during solid-state NMR measurements. Authors thank Prof. Rahul Banerjee (IISER Kolkata) for discussions. Authors acknowledge Dr. Vinayak Rane (TIFR) for help with EPR measurements. JD acknowledges DAE and start-up research grant from TIFR, India.

REFERENCES

1. O. G. Reid, R. D. Pensack, Y. Song, G. D. Scholes and G. Rumbles, *Chem. Mater.*, 2013, **26**, 561-575.
2. A. Listorti, B. O'Regan and J. R. Durrant, *Chem. Mater.*, 2011, **23**, 3381-3399.
3. A. J. Esswein and D. G. Nocera, *Chem. Rev.*, 2007, **107**, 4022-4047.
4. F. D'Souza, R. Chitta, A. S. D. Sandanayaka, N. K. Subbaiyan, L. D'Souza, Y. Araki and O. Ito, *J. Am. Chem. Soc.*, 2007, **129**, 15865-15871.
5. M. R. Wasielewski, *Acc. Chem. Res.*, 2009, **42**, 1910-1921.
6. T. R. Cook, Y. R. Zheng and P. J. Stang, *Chem. Rev.*, 2013, **113**, 734-777.
7. M. D. Ward and P. R. Raithby, *Chem. Soc. Rev.*, 2013, **42**, 1619-1636.
8. D. Ley, C. X. Guzman, K. H. Adolfsson, A. M. Scott and A. B. Braunschweig, *J. Am. Chem. Soc.*, 2014, **136**, 7809-7812.
9. V. Strauss, J. T. Margraf, K. Dirian, Z. Syrgiannis, M. Prato, C. Wessendorf, A. Hirsch, T. Clark and D. M. Guldi, *Angew. Chem., Int. Ed.*, 2015, **54**, 8292-8297.
10. P. Bujak, I. Kulszewicz-Bajer, M. Zagorska, V. Maurel, I. Wielgus and A. Pron, *Chem. Soc. Rev.*, 2013, **42**, 8895-8999.

11. A. W. Hains, Z. Liang, M. A. Woodhouse and B. A. Gregg, *Chem. Rev.*, 2010, **110**, 6689-6735.
12. G. R. Desiraju, *Accounts of Chemical Research*, 1996, **29**, 441-449.
13. F. Li, K. G. Yager, N. M. Dawson, J. Yang, K. J. Malloy and Y. Qin, *Macromolecules*, 2013, **46**, 9021-9031.
14. Z. Xiao, K. Sun, J. Subbiah, S. Ji, D. J. Jones and W. W. H. Wong, *Sci. Rep.*, 2014, **4**.
15. A. P. Cote, A. I. Benin, N. W. Ockwig, M. O'Keeffe, A. J. Matzger and O. M. Yaghi, *Science*, 2005, **310**, 1166-1170.
16. A. Comotti, S. Bracco, M. Mauri, S. Mottadelli, T. Ben, S. Qiu and P. Sozzani, *Angew. Chem., Int. Ed.*, 2012, **51**, 10136-10140.
17. S. Dalapati, R. Saha, S. Jana, A. K. Patra, A. Bhaumik, S. Kumar and N. Guchhait, *Angew. Chem., Int. Ed.*, 2012, **51**, 12534-12537.
18. S.-Y. Ding and W. Wang, *Chem. Soc. Rev.*, 2012, **42**, 548-568.
19. X. Feng, X. Ding and D. Jiang, *Chem. Soc. Rev.*, 2012, **41**, 6010-6022.
20. S. Kandambeth, A. Mallick, B. Lukose, M. V. Mane, T. Heine and R. Banerjee, *J. Am. Chem. Soc.*, 2012, **134**, 19524-19527.
21. S. Jin, X. Ding, X. Feng, M. Supur, K. Furukawa, S. Takahashi, M. Addicoat, M. E. El-Khouly, T. Nakamura, S. Irle, S. Fukuzumi, A. Nagai and D. Jiang, *Angew. Chem., Int. Ed.*, 2013, **52**, 2017-2021.
22. H. Oh, S. B. Kalidindi, Y. Um, S. Bureekaew, R. Schmid, R. A. Fischer and M. Hirscher, *Angew. Chem., Int. Ed.*, 2013, **52**, 13219-13222.
23. A. Dutta, K. Koh, A. G. Wong-Foy and A. J. Matzger, *Angew. Chem., Int. Ed.*, 2015, **54**, 3983-3987.
24. Y. Kubo, R. Nishiyabu and T. D. James, *Chem. Commun.*, 2015, **51**, 2005-2020.
25. H. Furukawa and O. M. Yaghi, *J. Am. Chem. Soc.*, 2009, **131**, 8875-8883.
26. D. D. Medina, V. Werner, F. Auras, R. Tautz, M. Dogru, J. Schuster, S. Linke, M. Doblinger, J. Feldmann, P. Knochel and T. Bein, *ACS Nano*, 2014, **8**, 4042-4052.
27. S. Duhovic and M. Dinca, *Chemistry of Materials*, 2015, **27**, 5487-5490.
28. H. B. Aiyappa, J. Thote, D. B. Shinde, R. Banerjee and S. Kurungot, *Chem. Mater.*, 2016, **28**, 4375-4379.
29. A. C. Jakowetz, T. F. Hinrichsen, L. Ascherl, T. Sick, M. Calik, F. Auras, D. D. Medina, R. H. Friend, A. Rao and T. Bein, *J. Am. Chem. Soc.*, 2019, **141**, 11565-11571.
30. N. C. Flanders, M. S. Kirschner, P. Kim, T. J. Fauvell, A. M. Evans, W. Helweh, A. P. Spencer, R. D. Schaller, W. R. Dichtel and L. X. Chen, *J. Am. Chem. Soc.*, 2020, **142**, 14957-14965.
31. S. Wan, J. Guo, J. Kim, H. Ihee and D. L. Jiang, *Angew. Chem., Int. Ed.*, 2008, **47**, 8826-8830.
32. S. Wan, J. Guo, J. Kim, H. Ihee and D. L. Jiang, *Angew. Chem., Int. Ed.*, 2009, **48**, 5439-5442.
33. X. S. Ding, L. Chen, Y. Honsho, X. Feng, O. Saenpawang, J. D. Guo, A. Saeki, S. Seki, S. Irle, S. Nagase, V. Parasuk and D. L. Jiang, *J. Am. Chem. Soc.*, 2011, **133**, 14510-14513.
34. X. S. Ding, J. Guo, X. A. Feng, Y. Honsho, J. D. Guo, S. Seki, P. Maitarad, A. Saeki, S. Nagase and D. L. Jiang, *Angew. Chem., Int. Ed.*, 2011, **50**, 1289-1293.
35. X. A. Feng, L. Chen, Y. P. Dong and D. L. Jiang, *Chem. Commun.*, 2011, **47**, 1979-1981.
36. X. S. Ding, X. Feng, A. Saeki, S. Seki, A. Nagai and D. L. Jiang, *Chem. Commun.*, 2012, **48**, 8952-8954.
37. X. Feng, L. Chen, Y. Honsho, O. Saengsawang, L. L. Liu, L. Wang, A. Saeki, S. Irle, S. Seki, Y. P. Dong and D. L. Jiang, *Adv. Mater.*, 2012, **24**, 3026-3031.
38. X. Feng, L. L. Liu, Y. Honsho, A. Saeki, S. Seki, S. Irle, Y. P. Dong, A. Nagai and D. L. Jiang, *Angew. Chem., Int. Ed.*, 2012, **51**, 2618-2622.
39. X. Chen, M. Addicoat, S. Irle, A. Nagai and D. L. Jiang, *J. Am. Chem. Soc.*, 2013, **135**, 546-549.

40. X. Feng, Y. P. Dong and D. L. Jiang, *CrystEngComm.*, 2013, **15**, 1508-1511.
41. S. B. Jin, X. S. Ding, X. Feng, M. Supur, K. Furukawa, S. Takahashi, M. Addicoat, M. E. El-Khouly, T. Nakamura, S. Irle, S. Fukuzumi, A. Nagai and D. L. Jiang, *Angew. Chem., Int. Ed.*, 2013, **52**, 2017-2021.
42. S. B. Jin, K. Furukawa, M. Addicoat, L. Chen, S. Takahashi, S. Irle, T. Nakamura and D. L. Jiang, *Chem. Sci.*, 2013, **4**, 4505-4511.
43. N. Huang, X. S. Ding, J. Kim, H. Ihee and D. L. Jiang, *Angew. Chem., Int. Ed.*, 2015, **54**, 8704-8707.
44. S. B. Jin, M. Supur, M. Addicoat, K. Furukawa, L. Chen, T. Nakamura, S. Fukuzumi, S. Irle and D. L. Jiang, *J. Am. Chem. Soc.*, 2015, **137**, 7817-7827.
45. D. D. Medina, J. M. Rotter, Y. H. Hu, M. Dogru, V. Werner, F. Auras, J. T. Markiewicz, P. Knochel and T. Bein, *J. Am. Chem. Soc.*, 2015, **137**, 1016-1019.
46. L. Chen, K. Furukawa, J. Gao, A. Nagai, T. Nakamura, Y. Dong and D. Jiang, *J. Am. Chem. Soc.*, 2014, **136**, 9806-9809.
47. T. W. Kim, S. Jun, Y. Ha, R. K. Yadav, A. Kumar, C.-Y. Yoo, I. Oh, H.-K. Lim, J. W. Shin, R. Ryoo, H. Kim, J. Kim, J.-O. Baeg and H. Ihee, *Nat. Commun.*, 2019, **10**, 1873.
48. J. Guo, Y. Xu, S. Jin, L. Chen, T. Kaji, Y. Honsho, M. A. Addicoat, J. Kim, A. Saeki, H. Ihee, S. Seki, S. Irle, M. Hiramoto, J. Gao and D. Jiang, *Nat. Commun.*, 2013, **4**.
49. A. Das, I. Mandal, R. Venkatramani and J. Dasgupta, *Sci. Adv.*, 2019, **5**, eaav4806.
50. A. Jha, D. Chakraborty, V. Srinivasan and J. Dasgupta, *J. Phys. Chem. B*, 2013, **117**, 12276-12285.
51. C. R. DeBlase, K. E. Silberstein, T. Thanh-Tam, H. D. Abruna and W. R. Dichtel, *J. Am. Chem. Soc.*, 2013, **135**, 16821-16824.
52. J. H. Chong, M. Sauer, B. O. Patrick and M. J. MacLachlan, *Org. Lett.*, 2003, **5**, 3823-3826.
53. C. V. Chandran, P. K. Madhu, N. D. Kurur and T. Brauniger, *Magn. Reson. Chem.*, 2008, **46**, 943-947.
54. M. Leskes, P. K. Madhu and S. Vega, *Chem. Phys. Lett.*, 2007, **447**, 370-374.
55. A. Jha, V. B. Yasarapudi, H. Jasbeer, C. Kanimozhi, S. Patil and J. Dasgupta, *J. Phys. Chem. C*, 2014, **118**, 29650-29662.
56. D. R. Armstrong, L. Balloch, E. Hevia, A. R. Kennedy, R. E. Mulvey, C. T. O'Hara and S. D. Robertson, *Beilstein J. Org. Chem.*, 2011, **7**, 1234-1248.
57. G. H. V. Bertrand, V. K. Michaelis, T.-C. Ong, R. G. Griffin and M. Dinca, *Proc. Natl. Acad. Sci. U.S.A.*, 2013, **110**, 4923-4928.
58. H. Zhu, N. Song and T. Lian, *J. Am. Chem. Soc.*, 2011, **133**, 8762-8771.
59. T. Fujisawa, M. Creelman and R. A. Mathies, *J. Phys. Chem. B*, 2012, **116**, 10453-10460.
60. R. Gera, A. Das, A. Jha and J. Dasgupta, *J. Am. Chem. Soc.*, 2014, **136**, 15909-15912.
61. A. Das, A. Jha, R. Gera and J. Dasgupta, *J. Phys. Chem. C*, 2015, **119**, 21234-21242.
62. M. Dogru, M. Handloser, F. Auras, T. Kunz, D. Medina, A. Hartschuh, P. Knochel and T. Bein, *Angew. Chem., Int. Ed.*, 2013, **52**, 2920-2924.
63. R. Englman and J. Jortner, *Mol. Phys.*, 1970, **18**, 145-164.
64. S. Albert-Seifried, D.-H. Ko, S. Huettner, C. Kanimozhi, S. Patil and R. H. Friend, *Phys. Chem. Chem. Phys.*, 2014, **16**, 6743-6752.
65. Z. Galus and R. N. Adams, *J. Chem. Phys.*, 1962, **36**, 2814.
66. R. L. Spicer, A. D. Stergiou, T. A. Young, F. Duarte, M. D. Symes and P. J. Lusby, *J. Am. Chem. Soc.*, 2020, **142**, 2134-2139.
67. T. Sick, A. G. Hufnagel, J. Kampmann, I. Kondofersky, M. Calik, J. M. Rotter, A. Evans, M. Döblinger, S. Herbert, K. Peters, D. Böhm, P. Knochel, D. D. Medina, D. Fattakhova-Rohlfing and T. Bein, *J. Am. Chem. Soc.*, 2018, **140**, 2085-2092.
68. S. Bi, C. Yang, W. Zhang, J. Xu, L. Liu, D. Wu, X. Wang, Y. Han, Q. Liang and F. Zhang, *Nat. Commun.*, 2019, **10**, 2467.

Figures and Legends

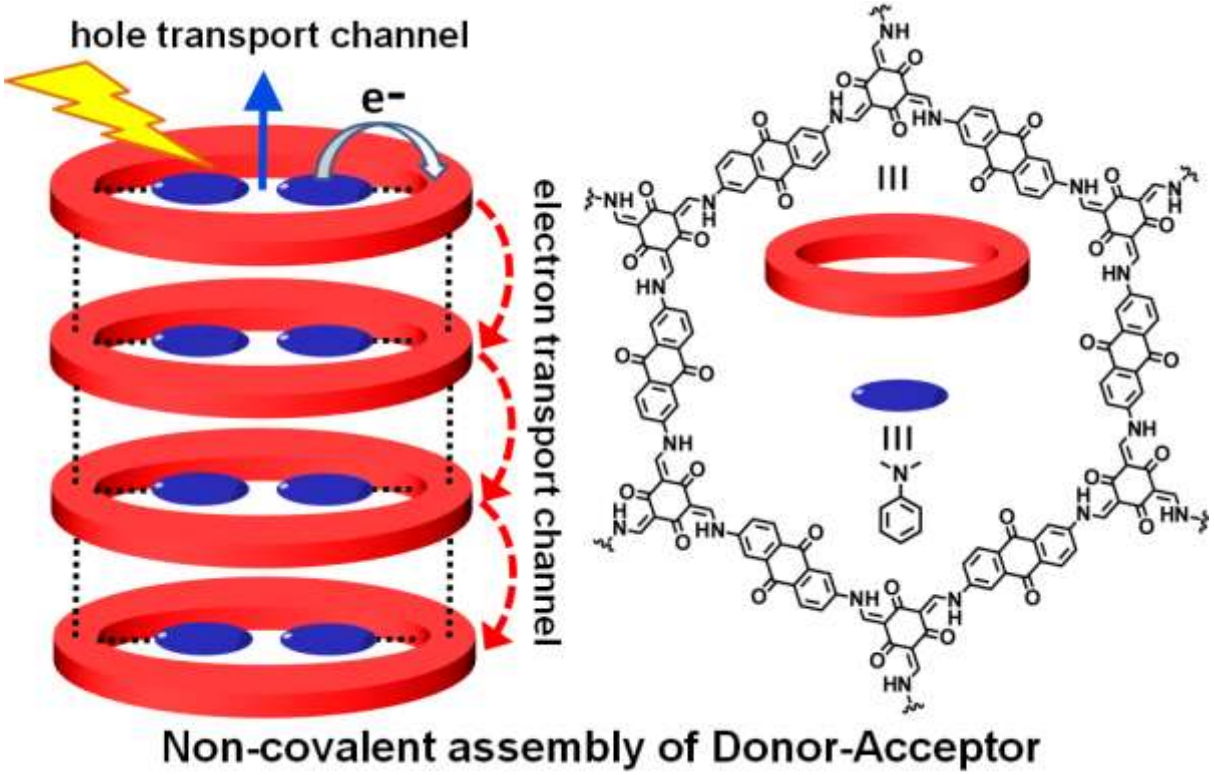

Figure 1. Conceptual representation of photoinduced charge generation with donor incarcerated inside a photoactive covalent organic framework (COF). Subsequent to excitation, electron transfer occurs from guest molecules to the host COF framework. Charge separation is achieved through different charge transport channels. (right) Chemical structure of the host DAAQ-TFP COF and the guest N,N-dimethylaniline (DMA).

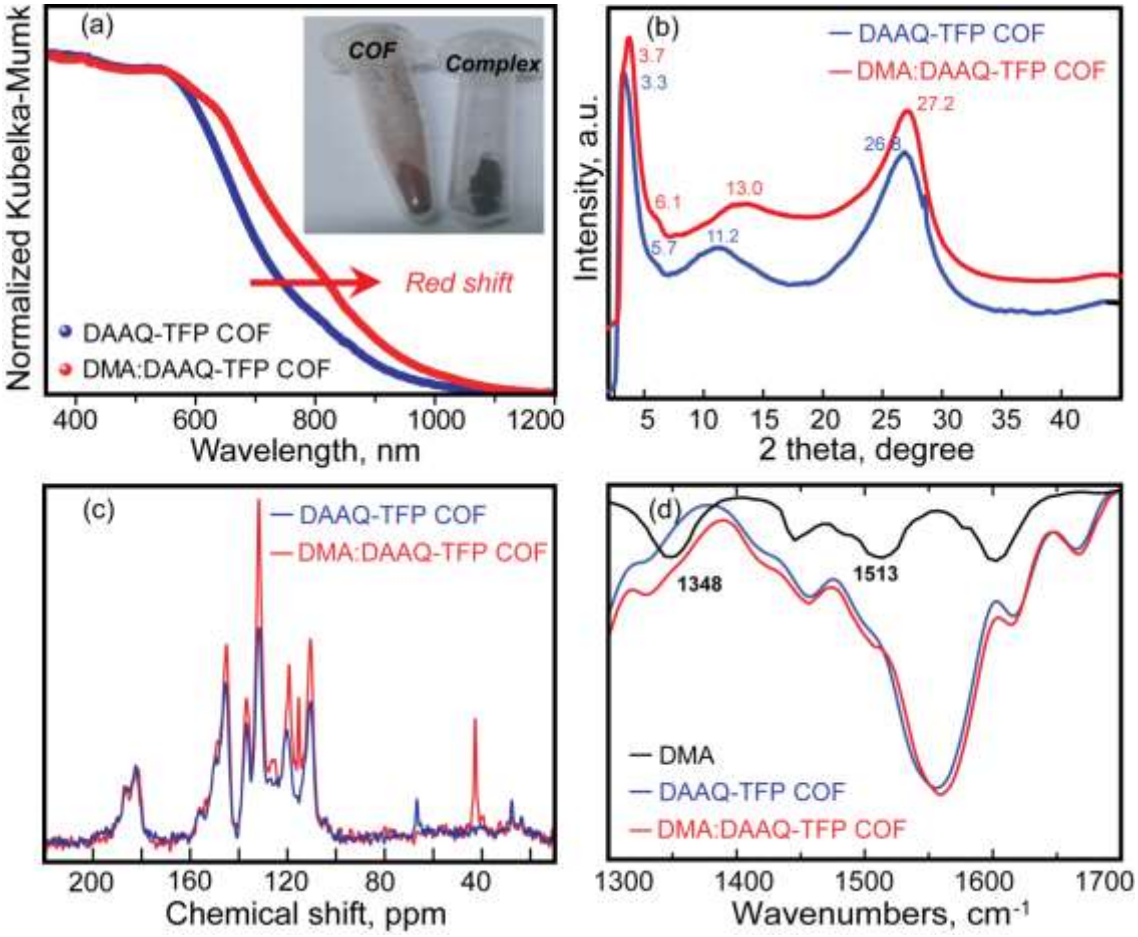

Figure 2. Characterization of DMA⊂DAAQ-TFP COF inclusion complex: (a) absorption spectra of DAAQ-TFP COF (blue) and DMA⊂DAAQ-TFP COF inclusion complex (red) obtained by diffuse reflectance. Inclusion complex shows a clear red shift in the absorption spectrum that changes the colour of the material from brick red to black. (b) Powder-XRD measurements. (c) Comparison of the solid state ^{13}C-NMR spectra of the complex with the COF only sample. Distinct peak of alkyl carbon at δ=40 ppm along with the new peaks in aromatic region confirms the inclusion of DMA. (d) Comparison of FTIR spectra of DAAQ-TFP COF with DMA and the inclusion complex.

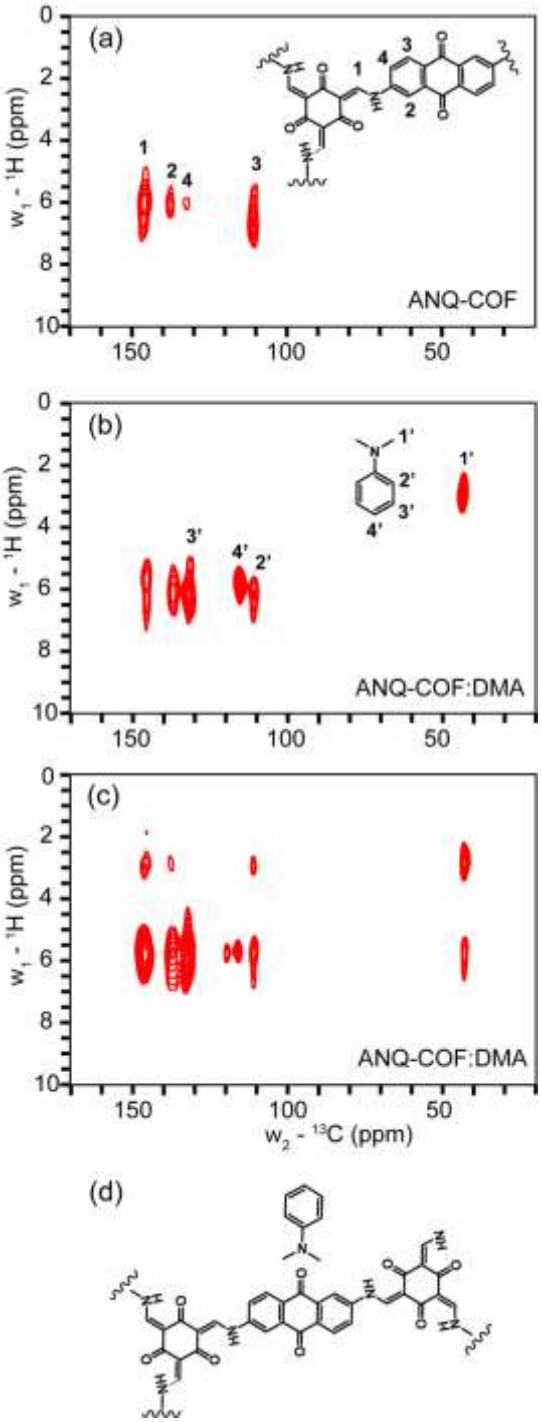

Figure 3. ^{1}H-^{13}C correlation solid-state NMR experiments: (a) DAAQ-TFP COF; (b) DMA⊂DAAQ-TFP COF; (c) DMA⊂DAAQ-TFP COF with an additional spin diffusion element to establish inter and intra-molecular correlations; and (d) proposed molecular arrangement in the photoactive assembly.

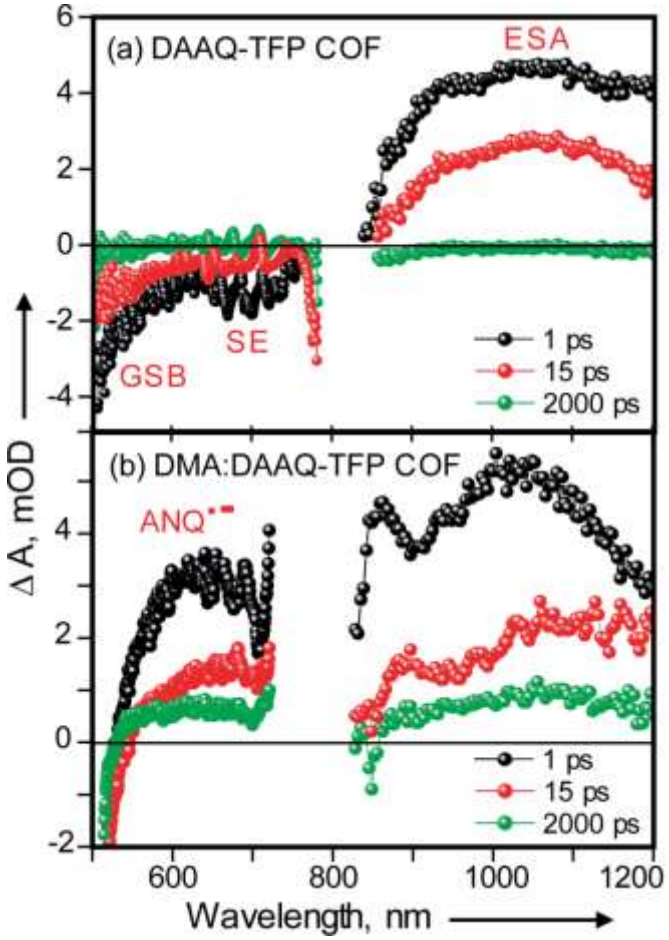

Figure 4. Transient absorption spectra obtained from films of (a) DAAQ-TFP COF and (b) DMA⊂DAAQ-TFP COF inclusion complex with λex = 490 nm. Inclusion complex shows a broad absorption feature at ~630 nm assigned to anthraquinone centric anion radical. Time resolution of the experiment was ~110 fs which was determined using optical Kerr experiment.

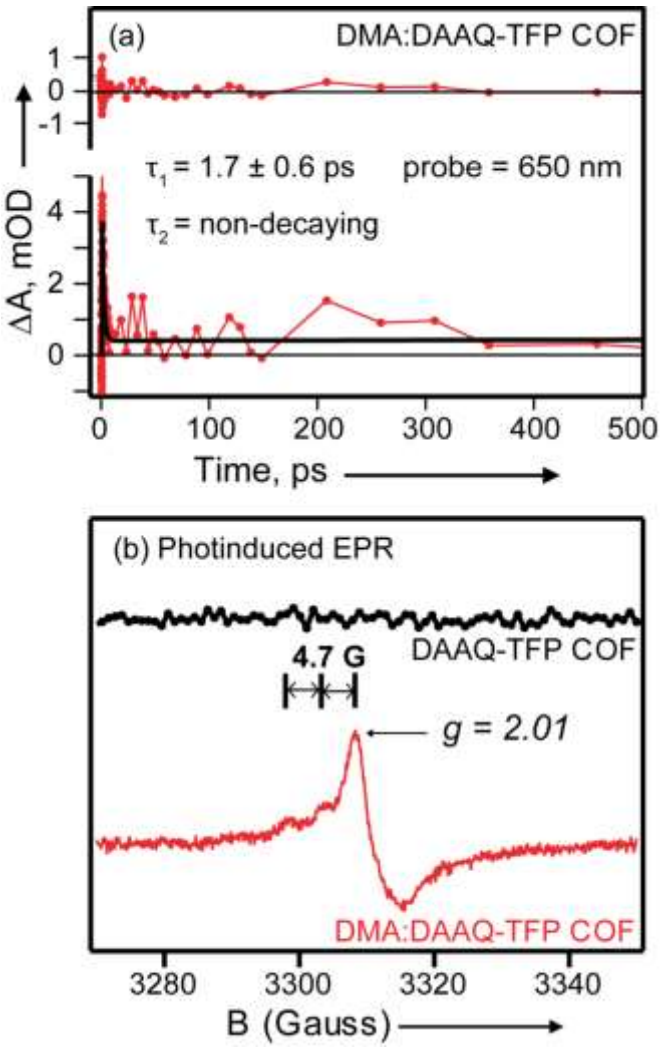

Figure 5. (a) Transient absorption kinetic trace obtained at probe wavelength = 650 nm for DMA⊂DAAQ-TFP COF inclusion complex clearly shows a fast decay component of 1.7 ps along with a non-decaying component; (B) Photoinduced EPR spectra of DAAQ-TFP COF and DMA⊂DAAQ-TFP COF inclusion complex after excitation with visible light source while samples were kept at room temperature.

SUPPORTING INFORMATION

Photoactive Anthraquinone-Based Host-Guest Assembly for Long-Lived Charge Separation.

Ajay Jha, Kaustubh R. Mote, Suman Chandra, Perunthiruthy K. Madhu and Jyotishman Dasgupta*

*Email: dasgupta@tifr.res.in

Table of Contents

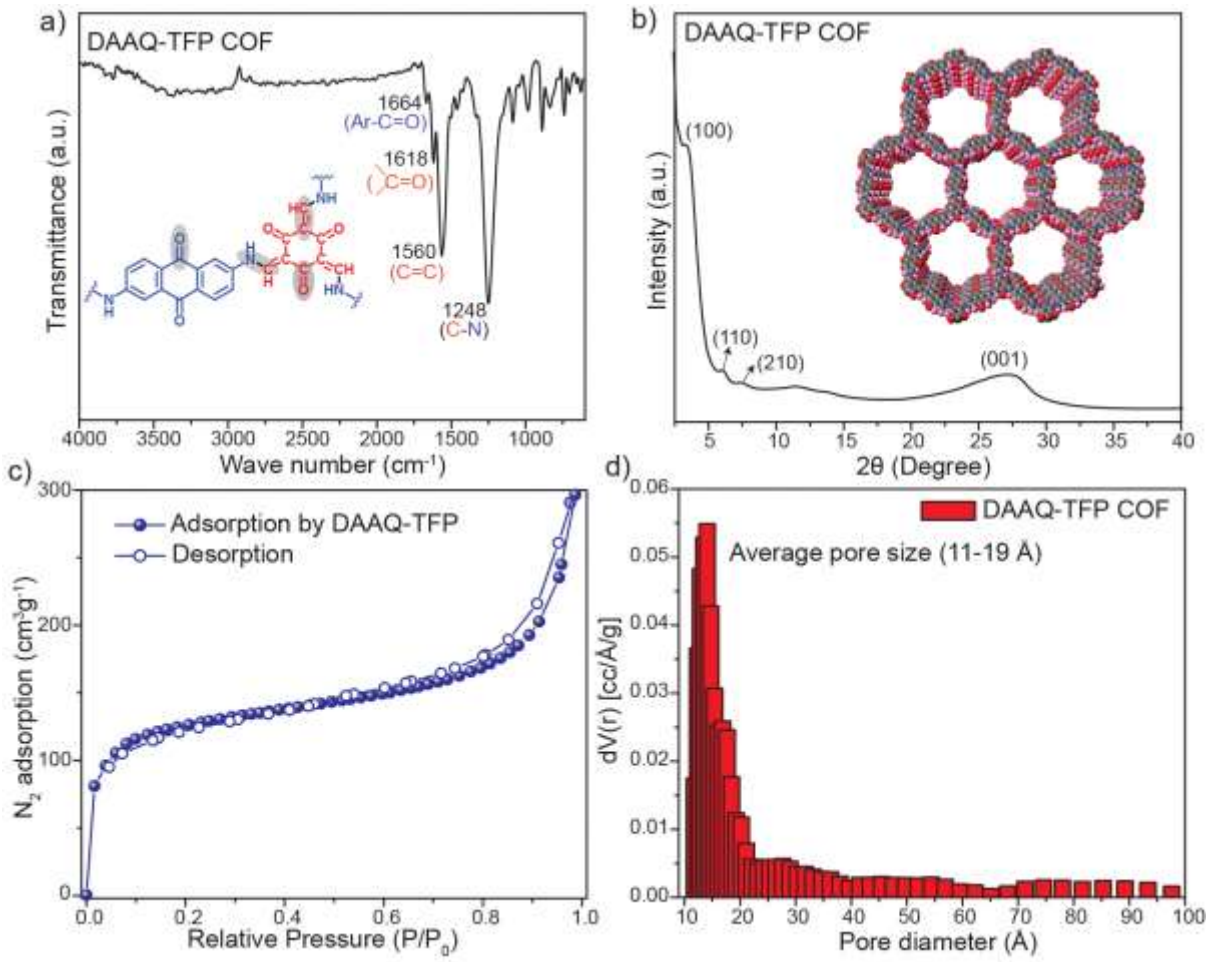

Figure S1. a) FTIR spectra with COF structure, b) PXRD with pore structure, c) Nitrogen absorption isotherms at 77 K and d) Pore size distribution of DAAQ-TFP COF.

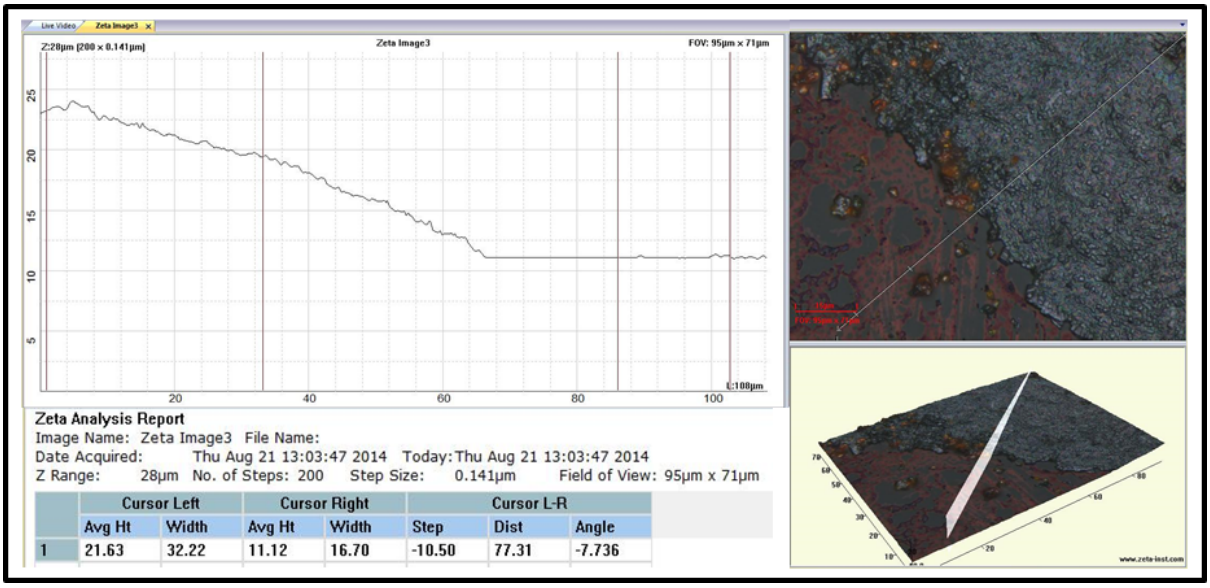

Figure S2. Film thickness characterization using Zeta microscopy set up.

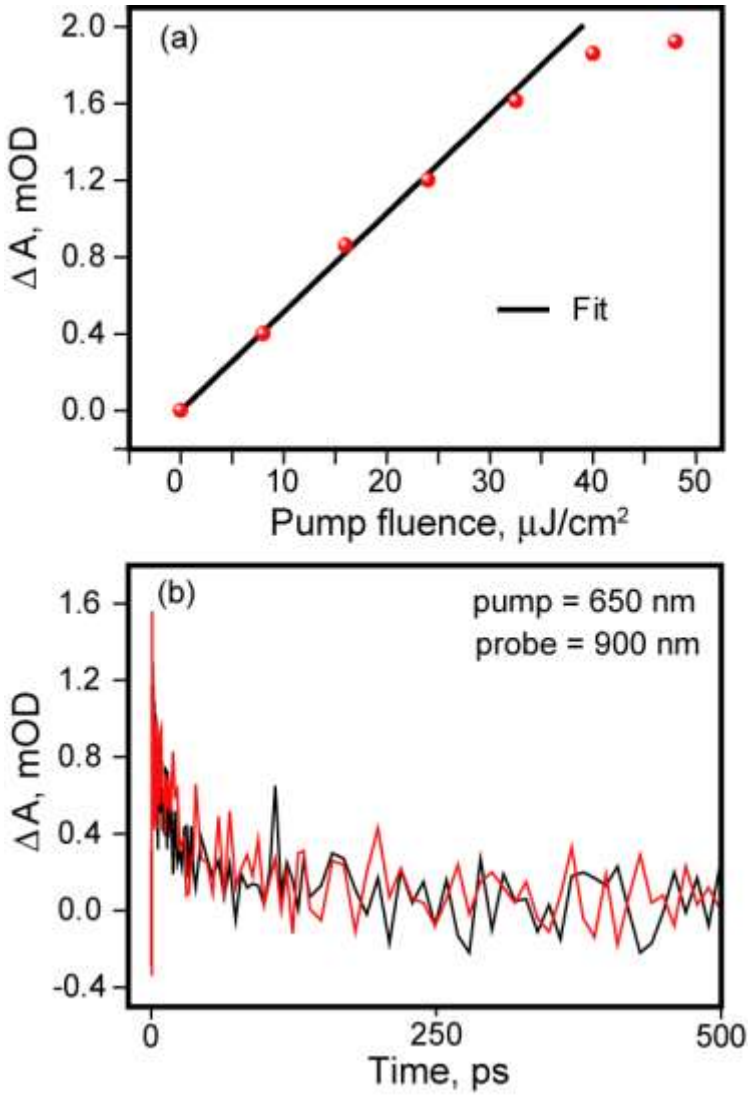

Figure S3. (a) Transient absorption signal amplitude of a neat DAAQ-TFP COF thin film at 900 nm, taken at 1 ps delay after the pump pulse with different pump fluence; (b) Excited state absorption kinetics at 900 nm probe wavelength for two different sets of measurements at the same spot after subjecting the samples to excitation at 490 nm.

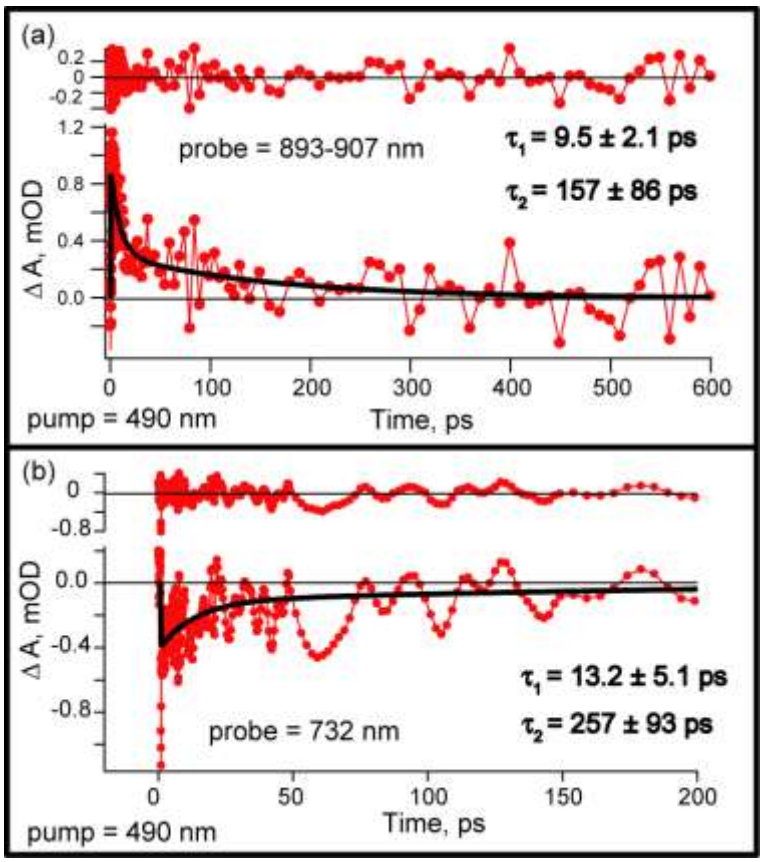

Figure S4. Transient absorption kinetic trace obtained at probe wavelength (a) 893-907 nm and (b) 732 nm for DAAQ-TFP COF thin film with λ_{ex} = 490 nm.

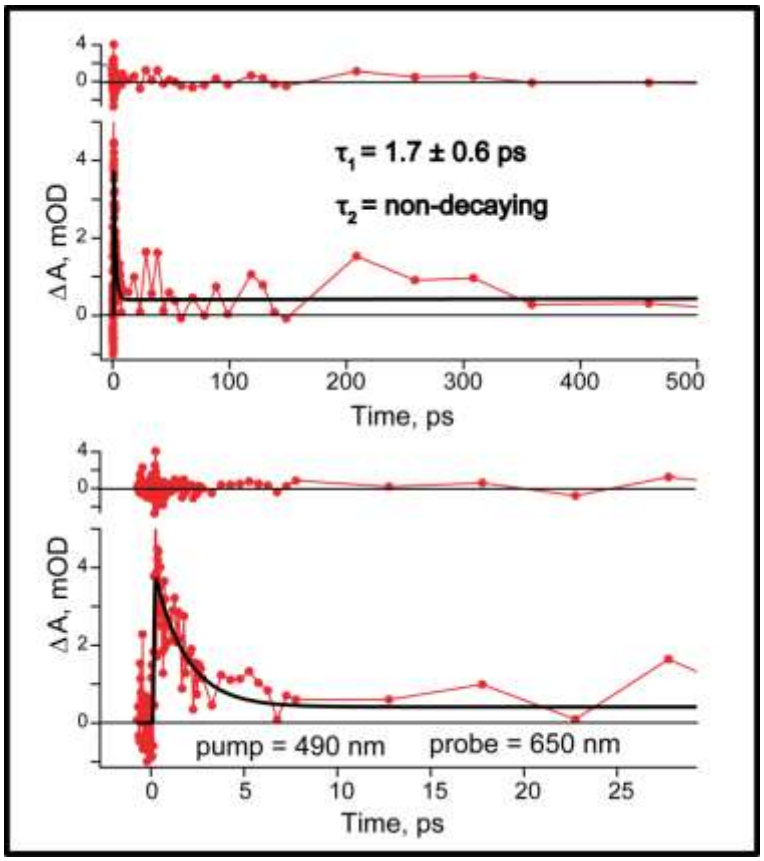

Figure S5. Transient absorption kinetic trace obtained at probe wavelength 650 nm for DMA⊂DAAQ-TFP COF inclusion complex thin film with λ_{ex} = 490 nm.

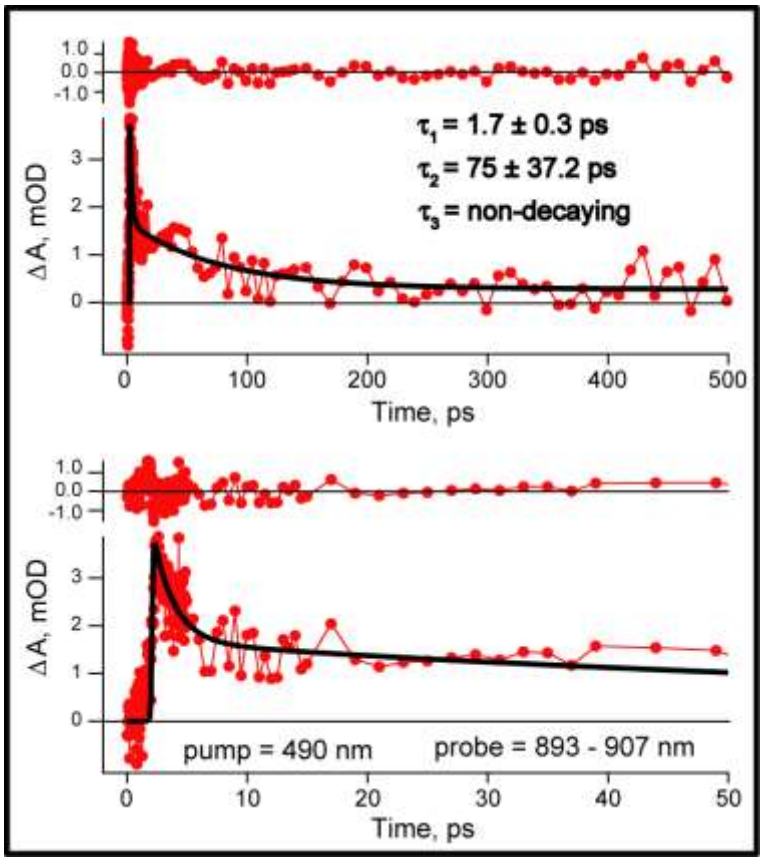

Figure S6. Transient absorption kinetic trace obtained at probe wavelength 893-907 nm for DMA⊂ DAAQ-TFP COF inclusion complex thin film with λ_{ex} = 490 nm.